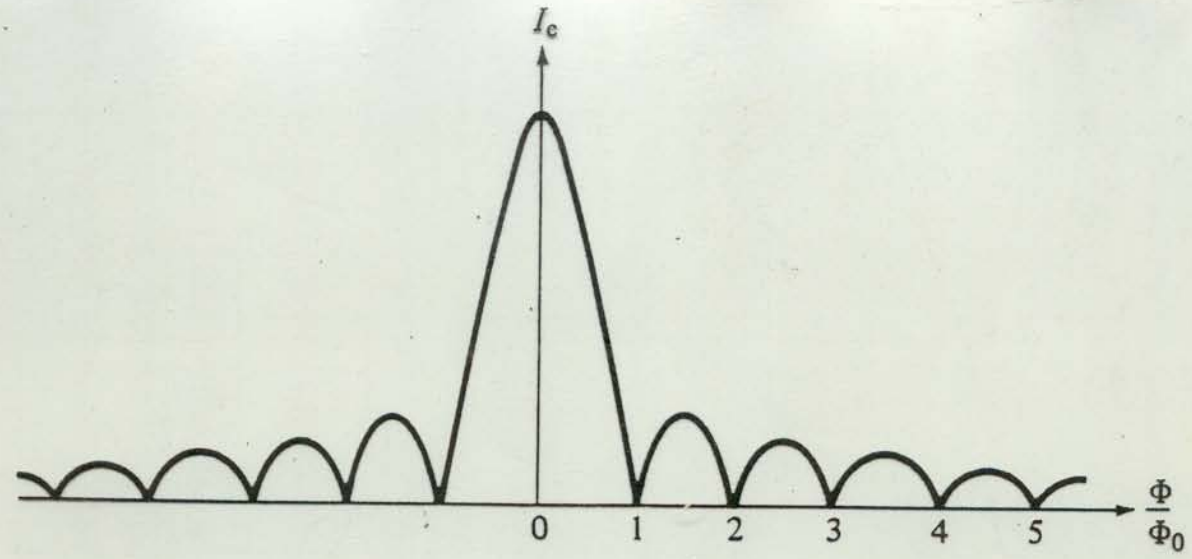

Figure 4.05d. Dependence of the maximum zero-voltage current in a junction with a current density of the form in Fig. 4.05c as a function of the flux linking the junction.

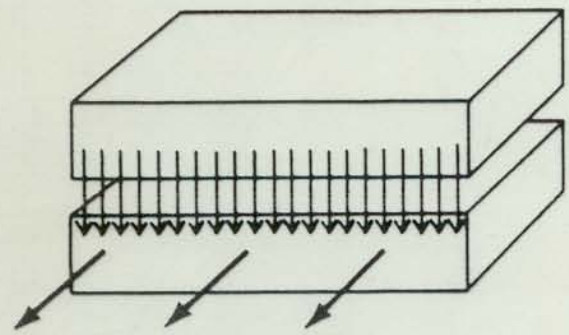

Magnetic flux = 0

(i)

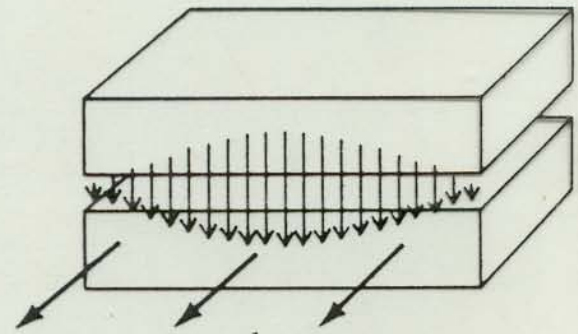

Magnetic flux = $\frac{1}{2}\Phi_0$

(ii)

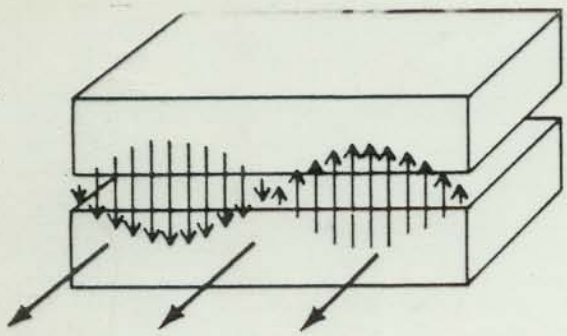

Magnetic flux = Φ_0

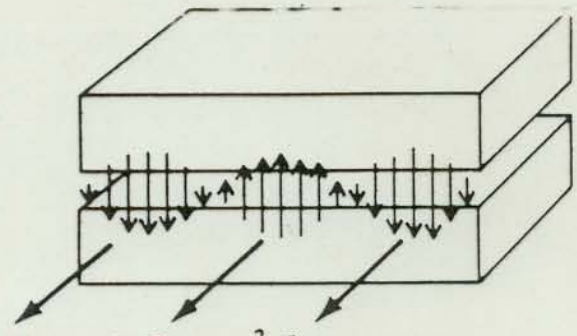

Magnetic flux = $\frac{3}{2}\Phi_0$

parallel to the surface, and the distance z_0 between the surface and the pickup loop is typically a few micrometers. Although z_0 is known approximately from the experimental setup, in practice the exact value of z_0 at low temperatures should be considered an unknown. We detect the change in the flux through the pickup loop while scanning the sample in x and y, so that the signal for each data set has an arbitrary constant offset. When the 8.2-μm pickup loop is used to image an anisotropic vortex in Tl-2201 (Fig. 1A), the interlayer spacing, $s = 11.6$ Å, and the a-axis penetration depth, $\lambda_a = 0.17$ μm (*15*), are both smaller than the spatial resolution. The interlayer penetration depth λ_c corresponds to currents flowing between the layers (along the c axis).

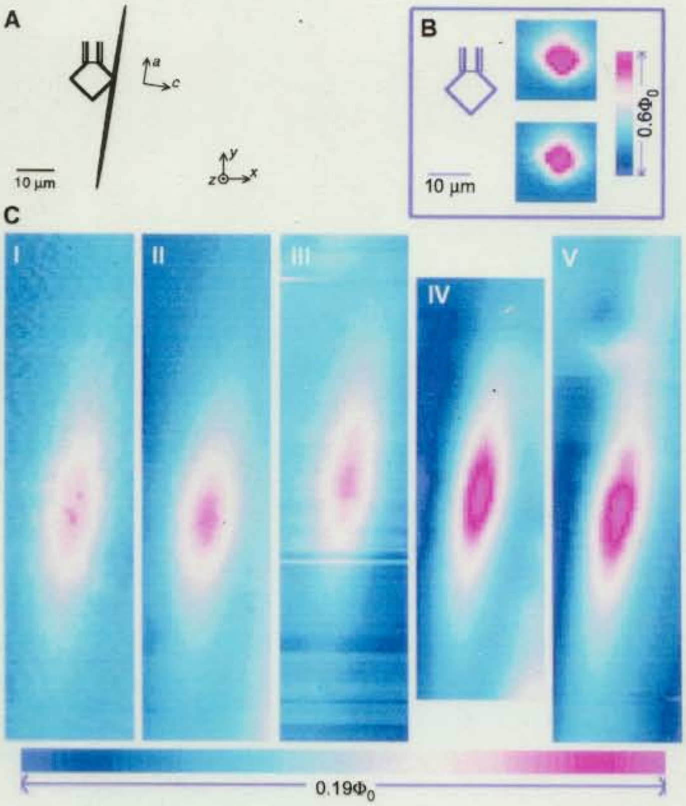

Fig. 1. (**A**) Sketch of an 8.2 μm by 8.2 μm pickup loop with shielded leads, together with a sketch of the magnetic fields of a highly anisotropic vortex. The flux through the pickup loop is given by the magnetic field B_z at a height $z_0 \approx 3$ μm, integrated over the area of the pickup loop; a and c indicate the $Tl_2Ba_2CuO_{6+\delta}$ crystal axes. The extent of the vortex along the a axis is called the c axis or interlayer penetration depth, because it is determined by supercurrents flowing between the layers, parallel to c. (**B**) For comparison, images of two $YBa_2Cu_3O_{6.95}$ *ab*-plane vortices. Because these vortices are much smaller than 8.2 μm, their apparent shape is dominated by the shape of the pickup loop. (**C**) Images of $Tl_2Ba_2CuO_{6+\delta}$ *ac*-plane vortices. Vortices I, II, and III were observed in crystal 1; vortices IV and V were observed in crystal 2. The vortices are resolution-limited in the c direction but extend tens of micrometers along the a axis, indicating qualitatively that λ_c is a few tens of micrometers.

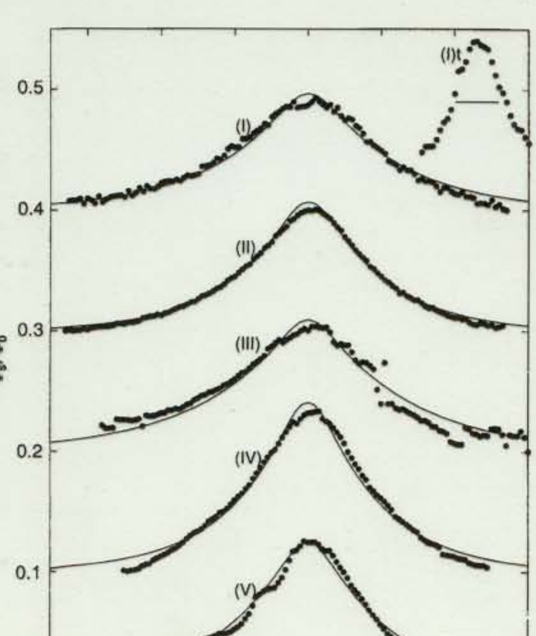

Fig. 2. Longitudinal cross sections along the a axis through the vortices from Fig. 1, plotted as the flux through the SQUID pickup loop, Φ_s (offset in $0.1\Phi_0$ increments) versus y. The data are fit to the functional form for the magnetic fields of an interlayer Josephson vortex with interlayer penetration depth λ_c, propagated to the height of the pickup loop above the surface, z_0, and integrated over the pickup loop. The fit parameters are: (I) $\lambda_c = 22^{+6}_{-4}$ μm, $z_0 = 3.0 \pm 0.6$ μm; (II) $\lambda_c = 18 \pm 2$ μm, $z_0 = 3.4 \pm 0.4$ μm; (III) $\lambda_c = 25^{+10}_{-7}$ μm, $z_0 = 2.0 \pm 1.0$ μm; (IV) $\lambda_c = 18 \pm 3$ μm, $z_0 = 2.2 \pm 0.6$ μm; and (V) $\lambda_c = 22^{+11}_{-7}$ μm, $z_0 = 1.9 \pm 1.0$ μm. A transverse cross section along x is also shown, with a scale bar indicating the extent of the pickup loop along x, 11.6 μm. The weighted average of the penetration depths is $\lambda_c = 19 \pm 2$ μm.

We have previously imaged vortices in niobium films (*14*) and *ab*-plane vortices in $YBa_2Cu_3O_{7-\delta}$ (YBCO) films (*12*) and crystals (*16*). In these cases, the relevant penetration depths are much smaller than the size of the pickup loop, so the vortices are well approximated by monopole sources of magnetic flux (*17*, *18*). Figure 1B shows images of two *ab*-plane vortices in YBCO, whose apparent shapes are determined by the shape of the pickup loop (*19*). In contrast, the interlayer vortices observed in images of the *ac* face of Tl-2201 (Fig. 1C) extend a considerable distance along the layers.

The Tl-2201 crystals were grown under carefully controlled conditions (*20*). The crystals we chose for these experiments were platelet-shaped, with a basal plane area of ~1 mm^2 and a thickness along the c axis varying between 50 and 100 μm. The images were made in a magnetically shielded dewar with an unknown residual field of several milligauss. We observed many similar *ac*-plane vortices in different parts of the two crystals. Five vortices (Fig. 1C) were chosen for detailed analysis because of their relatively large spacing from neighboring vortices. The vortices extend a few tens of micrometers along the a axis, indicating qualitatively that λ_c is a few tens of micrometers. The full width at half-maximum (FWHM) along the a axis ranged from 35 to 46 μm (Fig. 2).

Neglecting the influence of the surface on the fields, and defining a and c as the directions parallel and perpendicular to the layers, respectively, the z-component of the magnetic field of an interlayer Josephson vortex is given by

$$b_z(x_c, y_a, z = 0) = \frac{\Phi_0}{2\pi\lambda_a\lambda_c} K_0(\tilde{R}) \qquad (3)$$

(*10*), where

$$\tilde{R} = [(s/2\lambda_a)^2 + (x_c/\lambda a)^2 + (y_a/\lambda c)^2]^{1/2} \qquad (4)$$

K_0 is a modified Bessel function of the second kind (of order 0), and x_c and y_a denote the distance along the c axis and a axis, respectively (*11*). In our images, the crystal axes are rotated by 9° from the scan axes (Fig. 1). For these experiments, $\lambda_a \ll (L, \lambda_c)$, so it is appropriate to integrate over x_c at the surface. After this integration, the FWHM along y_a is $\sqrt{2}\lambda_c$. For